5. High Time Resolution Astrophysics (HTRA)

WHY HIGH TIME RESOLUTION?

High Time Resolution Astronomy/Astrophysics (HTRA) concerns itself with observations on time scales of a few seconds or less. In this regime there are a number of known fundamental science questions that can only be addressed using HTRA methodologies.

- lunar and planetary occultations
- transits of extra-solar planets
- eclipses and jets in accreting systems
- rapid and quasi-periodic variability (in the range 1-1000 Hz) in X-ray binary systems
- timing of isolated neutron stars

These studies require specialised equipment and high photon rates (i.e. efficient detectors and large area telescopes).

TECHNIQUES IN HTRA: POWER SPECTRAL ANALYSIS

The *rapid* flux variability of a (binned) light curve is studied using Fourier tecniques, that is exploiting the decomposition of the signal in Fourier components. A fundamental tool is provided by the Power Density Spectrum (PDS), defined as the *sum of the square modulus of the Fourier components of a signal*.

Any discrete signal (time series) can be written as the sum of complex exponentials in the frequency domain:

$$f(t_j) = \frac{1}{N} \sum_{k=1}^{N} a_k e^{-i\omega_k t_j} \tag{1}$$

where t_j denotes a time bin and $\omega_k = 2\pi\nu_k$ a frequency bin.

- The terms a_k are known as Fourier coefficients (or amplitudes), and can be found by means of a Fourier transform (usually a FFT). They are complex-valued, containing an amplitude and phase
- Parseval theorem: $\sum_j (f(t_j) - < f >)^2 = (1/N) \sum_k |a_k|^2$

  The total variance $\sum_j (f(t_j) - < f >)^2 = N\sigma^2(f)$ of the light curve in the time domain is equal to the mean of the squared values of its Fourier coefficients
- These squared values are known as Fourier powers, and the set of all Fourier powers is a POWER DENSITY SPECTRUM (PDS)

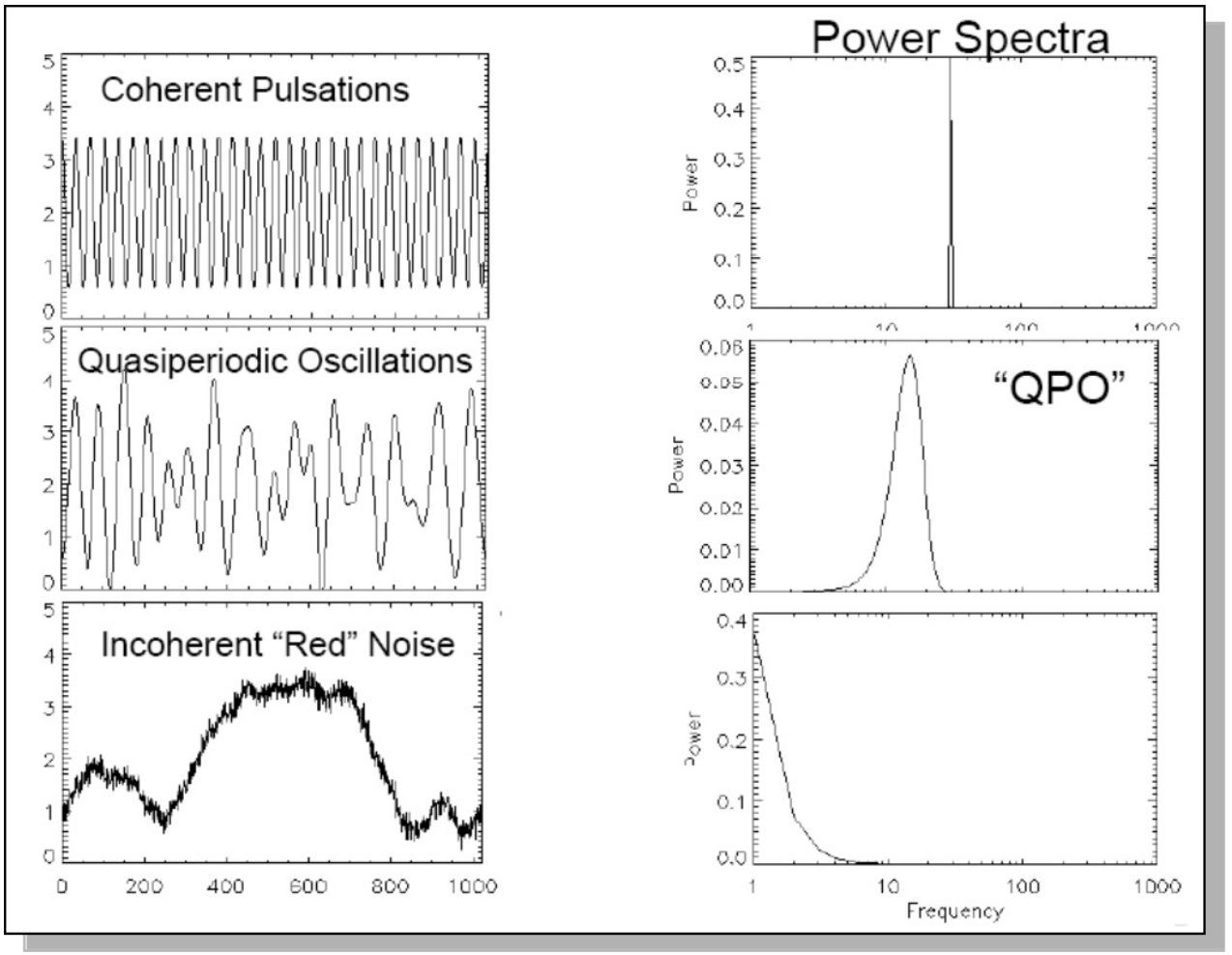

- Spike in the PDS (Fourier transform of a sine wave) $\Longrightarrow$ periodic (sinusoidal) signal
- Finite-width peak in the PDS $\Longrightarrow$ Quasi Periodic Oscillations (QPOs) in the signal

  Characterized observationally by:

  - centroid frequency ν_{QPO}

- frequency width (at FWHM) $\Delta\nu_{QPO}$
- quality value $Q = \nu_{QPO}/\Delta\nu_{QPO}$: signals with $Q > 2$ are called QPOs (those with $Q < 2$ peaked noise)
- coherence time $\tau = 1/(\pi\Delta\nu_{QPO})$

QPOs may be produced by different types of variability (e.g. a oscillation with varying frequency, exponentially damped sinusoid $e^{-t/\tau}\cos(2\pi\nu_0 t)$)

➠ continuum components in the PDS $\Longrightarrow$ noise

When dealing with noise one also needs to account for any possible instrument-induced noise.

Signal-to-noise of a weak QPO (or peaked noise) component (van der Klis 1989, 1998):

$$n_\sigma = 0.5 N_X r^2 (T/\Delta\nu_{QPO})^{1/2} \tag{2}$$

where N_X is the count rate, T the observing time (assumed $\gg 1/\Delta\nu_{QPO}$) and r the rms of the QPO (standard deviation of the light curve in the frequency range $\Delta\nu_{QPO}$)

TECHNIQUES IN HTRA: EPOCH FOLDING

- Epoch folding of an (unbinned) time series consists in calculating the phase of a photon with respect to a reference folding period T_f (removing the integer part) and then summing all the photons in the same phase bins. Another way to see it is to divide a (binned) light curve in intervakls of length T_f and then summing them.

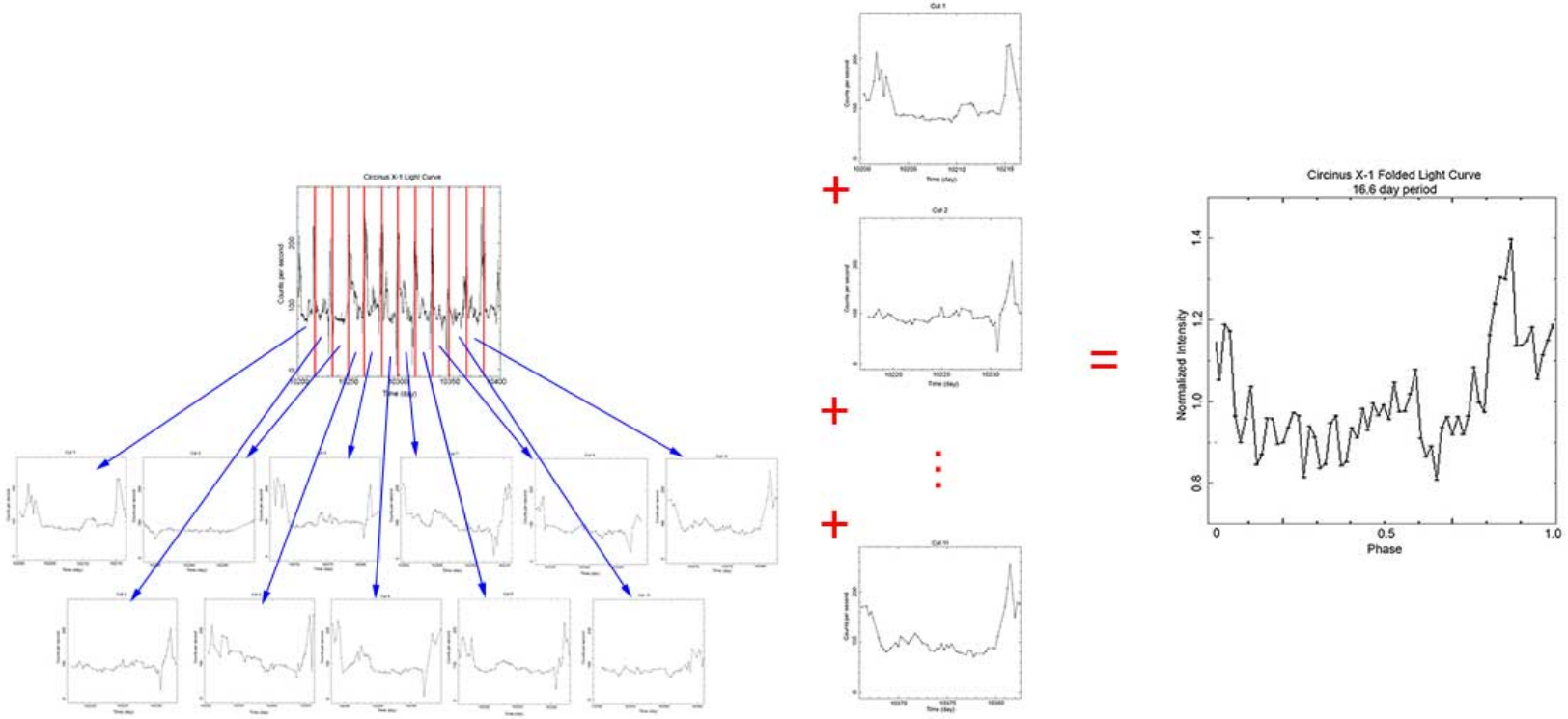

Figure 1: Light curve of X-ray binary system Circinus X-1 cut into 16.6 day segments. The individual 16.6-day light curves are summed into a single light curve covering just 16.6 days. If the chosen period is close to the period of variation for the object, the folded light curve will show a peak. (Credit: NASA's Imagine the Universe. https://imagine.gsfc.nasa.gov/science/toolbox/timing2.html)

Folding over T_f

$$\tau_i = t_i - \mathrm{int}(t_i/T_f)T_f \qquad 0 \leq t_i \leq T \tag{3}$$

$$\phi_i = \tau_i/T_f \qquad 0 \leq \phi_i \leq 1 \qquad \text{phase of photon} \tag{4}$$

Fortran code

```
do i=1,npt
read(2,*) ttfr
cntd=86400.0d0*ttfr
cnph=mod(cntd,period)
kfl=1
do k=1,nbins
if(cnph-vtph(k)>=0) kfl=k+1
enddo
vlcph(kfl)=vlcph(kfl)+1.0d0
if(i.eq.1) cntd1=cntd
if(i.eq.npt) cntd2=cntd
enddo
```

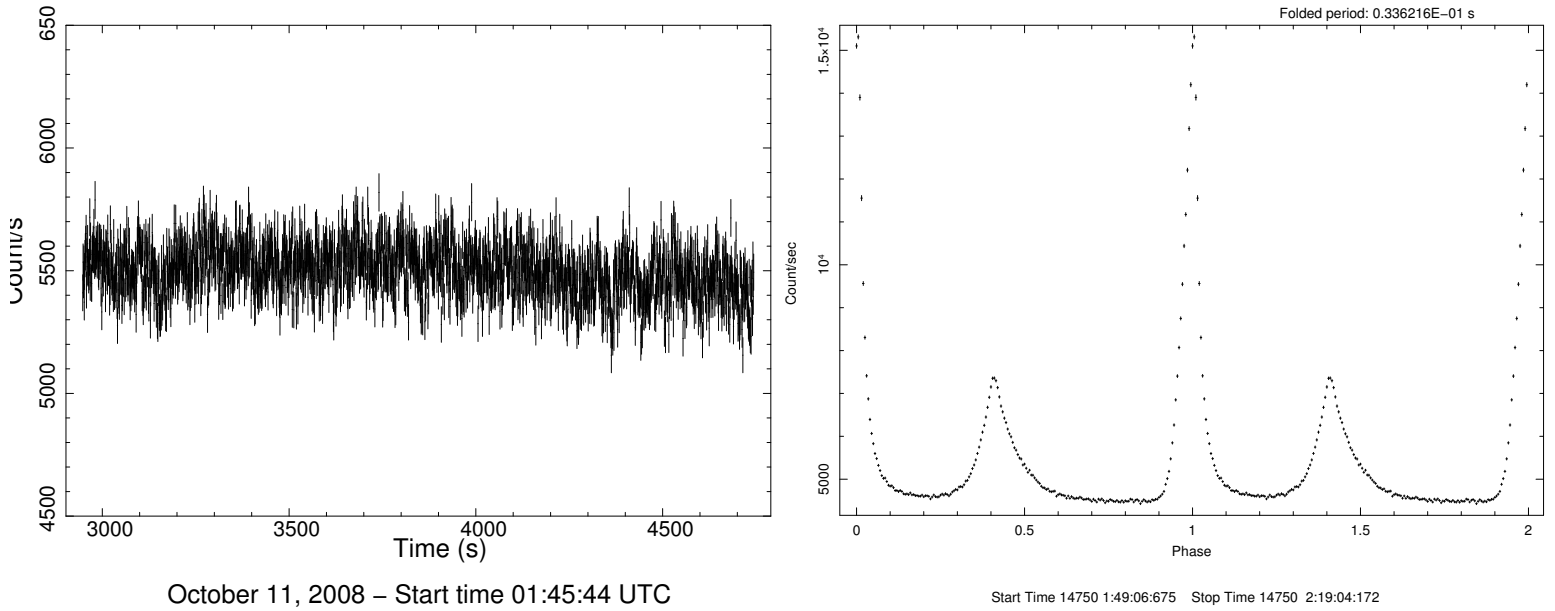

Figure 2: Binned time series (left) and folded times series (right) of the Crab pulsar (data taken with Aqueye). The folding period is $T_f = 0.0336216$ s.

- **Period search through chi2 maximization**

  Let's y_j be a folded and binned time series (with N_b phase bins). We fold it using several trials values of T_f. We then test the folded time series for constant behaviour using the χ^2 ($\nu = N_b - 1$ dof):

$$\chi^2 = \sum_{j=1}^{\nu} \left(\frac{y_j - \bar{y}}{e_j} \right)^2 \tag{5}$$

  – If T_f is wrong, $\chi^2 \simeq N_b - 1$ as the y_j's do not sum up in phase

– If T_f is correct, $\chi^2 >> N_b - 1$ as the y_j's sum up in phase and the resulting folded time series deviates significantly from a constant
Best period $T_{f,max} \rightarrow$ maximum of $\chi^2(T_f)$

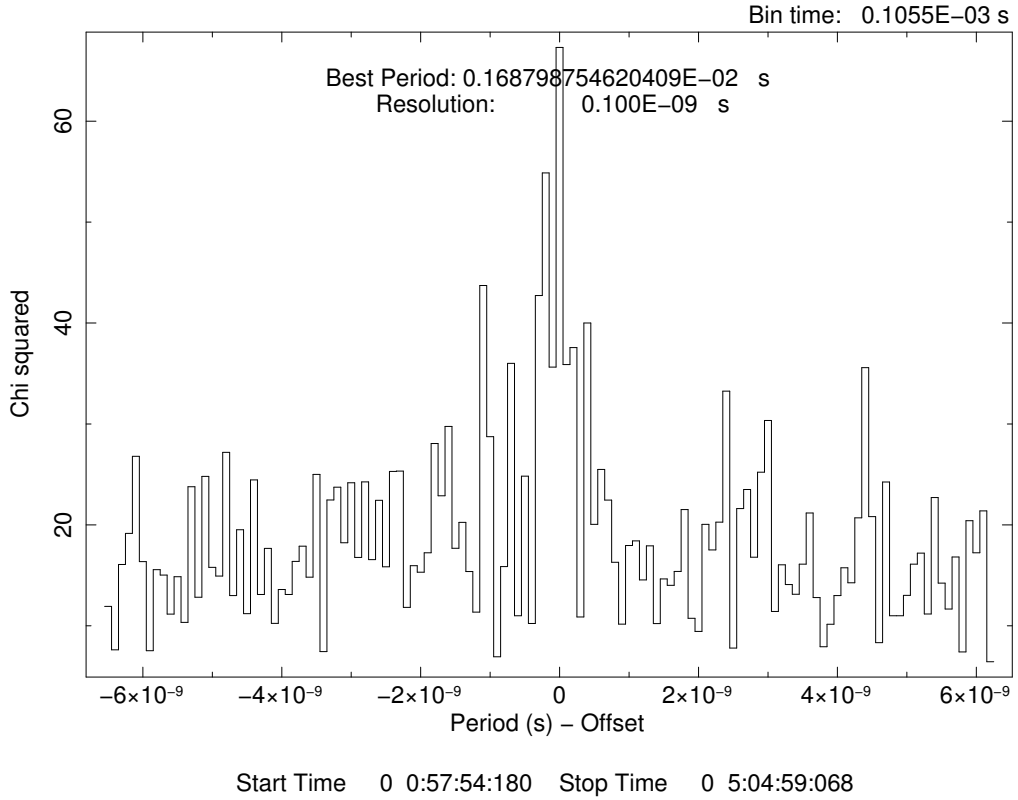

Figure 3: Epoch folding search of the rotational period of PSR J1023+0038 in January 25, 2018 (Aqueye+@Copernicus).

- **Folded profile: shape, amplitude and phase**

  Accurate studies of the folded profile allow us to determine its shape and the phase of any feature in it

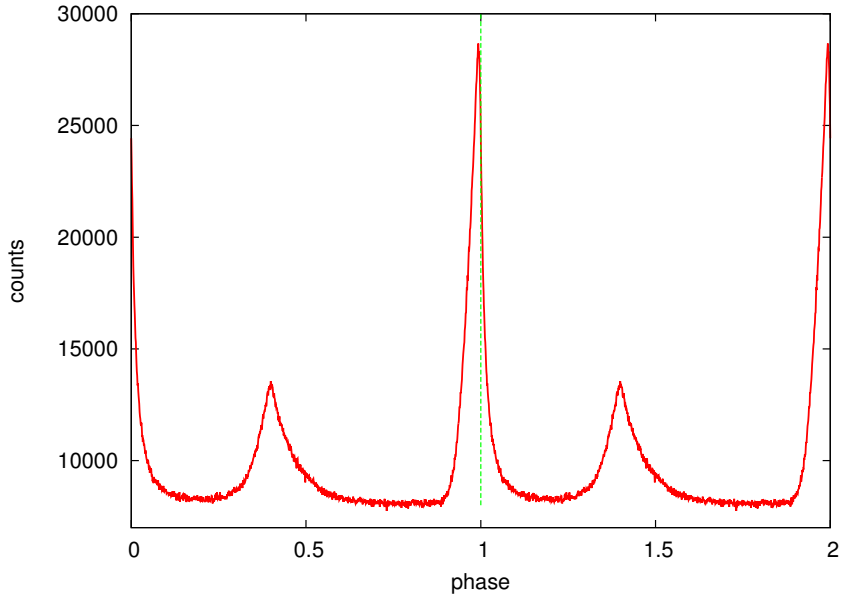

Figure 4: Folded light curve of the Crab pulsar as a function of phase. The folding period is 0.0336216417 s. For clarity two rotations of the neutron star are shown. Phase zero/one corresponds to the position of the main peak in the radio band and is marked with a vertical dashed line.

TECHNIQUES IN HTRA: PHASE FITTING

- Modelling the folded profile (analytically, numerically) $\rightarrow$ determining the phase of the main peak or other feature
- Plot and fit phase vs time. Modelling (with a polynomial) provides a phase coherent timing solution

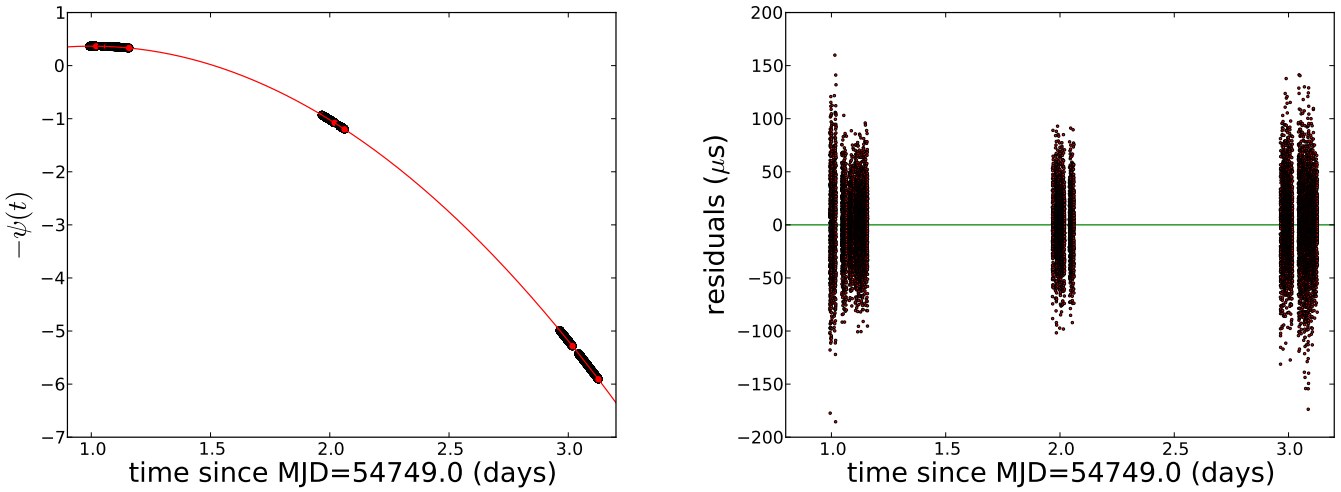

Figure 5: Left: phase drift of the main peak of the Crab pulsar (opposite sign). The (red) curve is the best-fitting parabola. The NS is spinning down. Right: phase residuals (in μs) after subtracting the best-fitting parabola from the phase-drift (Germaná et al. 2012).

- Accurate determination of the rotational frequency and period and, if statistics is sufficient, of frequency and period first (and possibly second) derivative.

Barycentric corrections of time series

- Travel delays on photon arrival times from source caused by several effects
- Corrections must be applied, usually referring to an observer at the solar system, whose clock is synchronized with that of a distant inertial observer

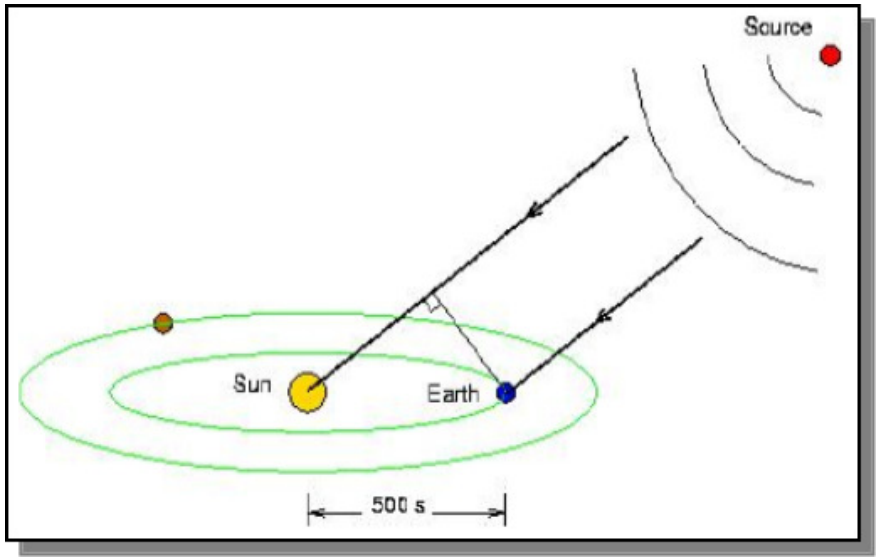

- For accurate timing, TEMPO and TEMPO2 are needed (Hobbs et al. 2006; Edwards et al. 2006) $\rightarrow$ account for special and general relativistic effects on the photon trajectory and clocks in the Solar system potential

LUNAR OCCULTATIONS

Lunar Occultations occur when the lunar limb passes in front of a star (or another celestial object).

The diffraction pattern (intensity distribution) of a plane wave of monochromatic light (wavelength λ) caused by the passage through a circular aperture of radius a is given by (Airy disc, Fig. 1 left):

$$I(\theta) = I_0[2J_1(2\pi(a/\lambda)\sin\theta)/(2\pi(a/\lambda)\sin\theta)]^2\,, \tag{6}$$

where J_1 is the (first order) Bessel function.

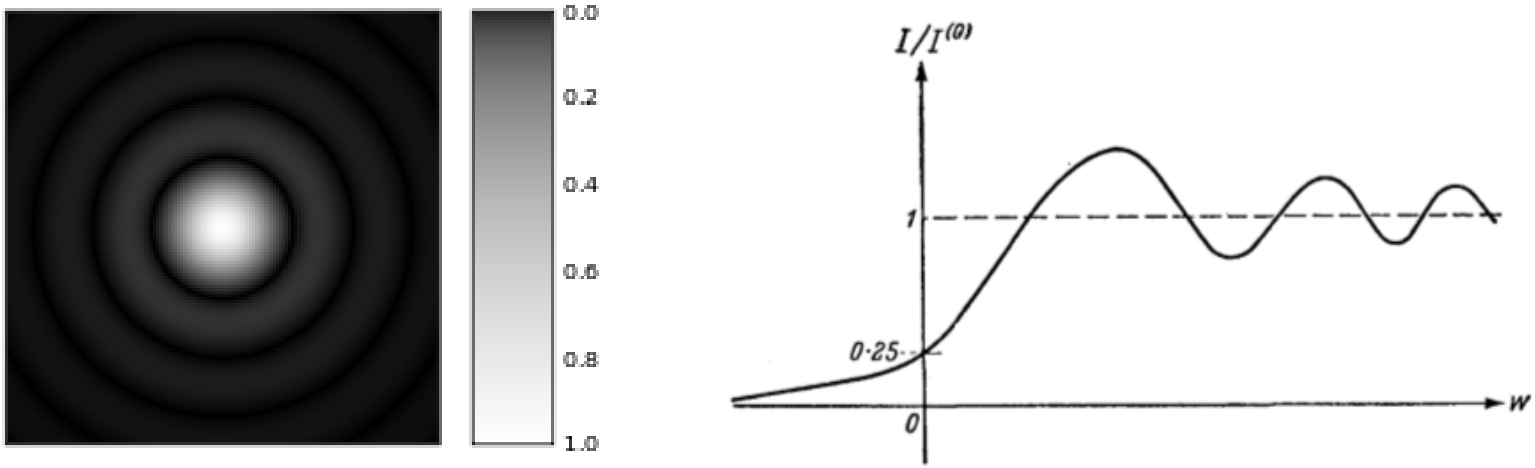

Figure 6: *Left*: Diffraction pattern of a circular aperture (Airy disc; source wikipedia). *Right*: Diffraction pattern of a sharp edge (Born & Wolf 1970, Fig. 8.39).

Similarly, light passing close to a straight edge undergoes diffraction. For a point-like source the

resulting pattern is (Born & Wolf 1970, Fig. 1 right):

$$I(\theta) = I_0/2\left[(1/2 + C(w))^2 + (1/2 + L(w))^2\right], \tag{7}$$

where $C(w)$ and $L(w)$ are known as Fresnel integrals, and $w = (2D_L/\lambda)^{1/2}\tan\theta$. D_L is the Moon distance.

For an extended source with brightness profile $S(\theta, \lambda)$, the diffraction pattern has to be integrated over θ and λ taking into account the total (telescope+filters+detector) wavelength response of the system ($\Lambda(\lambda)$).

This gives a total diffraction pattern which, because of the Moon motion, is a function of time ($I(t)$). The 'diffraction shadow' sweeps through the telescope at the apparent Moon speed $V_L \sim 1000$ m/s. Fitting $I(t)$ with a model for $S(\theta, \lambda)$ provides the physical parameters of the star.

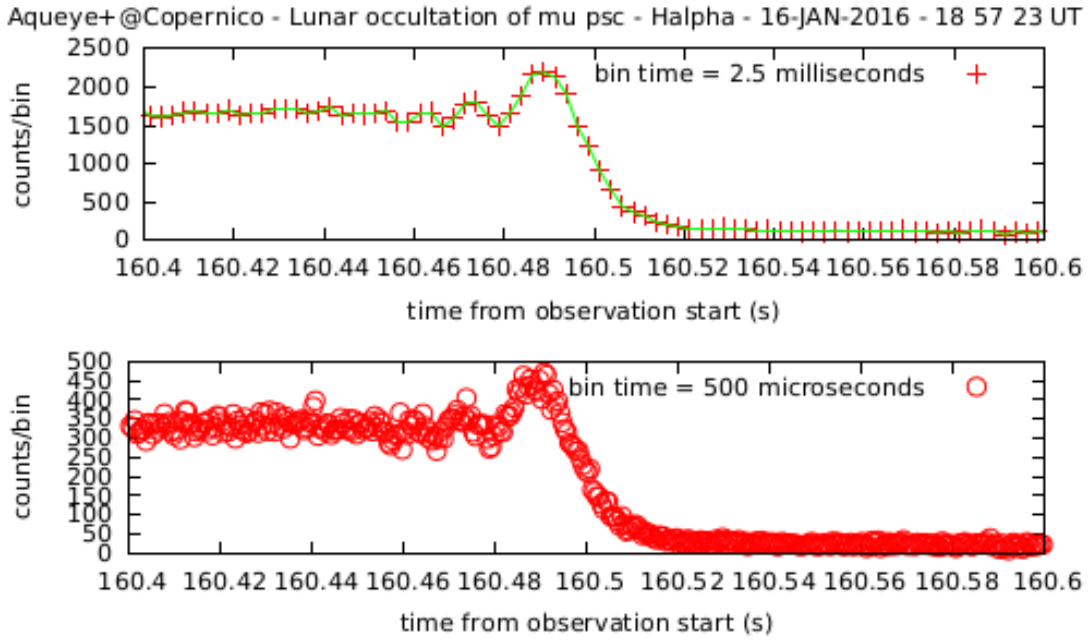

Figure 7: Lunar occultation of μ psc with Aqueye+@Copernico (Halpha filter, 16-JAN-2016, 18 57 23 UT).

The inferred apparent diameter of the star is: 3.14 ± 0.05 mas.

RAPID VARIABILITY IN BINARY SYSTEMS

Short-term variability in XRBs usually observed in the range *from 10-100 mHz up to 1 kHz*: slower variations usually studied in the time-domain (as on longer time scales source-state changes and data gaps cause trouble for Fourier techniques); faster variations not (yet) detected

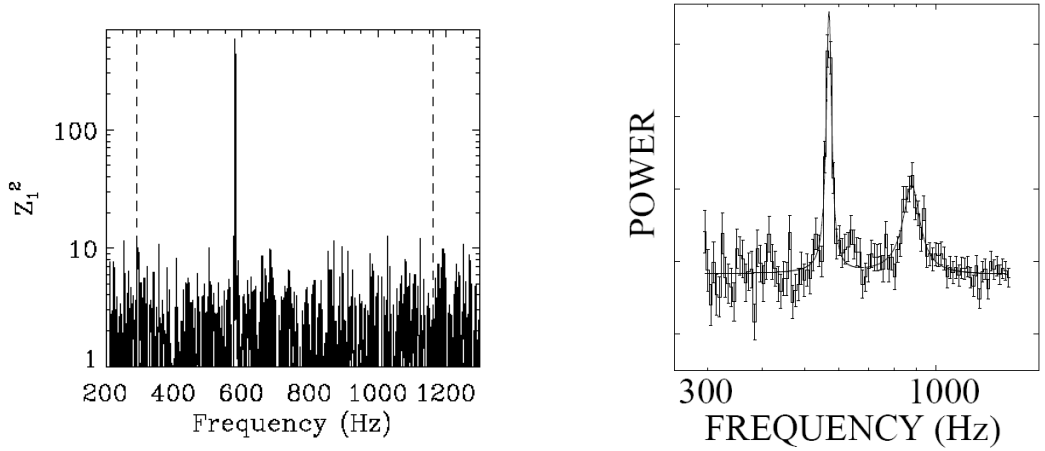

Figure 8: *Left*: periodic oscillation (burst oscillation) in the PDS of 4U 1636-53 (from Strohmayer 1999). *Right*: Quasi Periodic Oscillations (kHz QPOs) in the PDS of 4U1608-52 (Mendez et al. 1998).

Rapid variability in XRBs

The rapid (100-1000 Hz) variability phenomena observed in X-ray binaries are essentially of five types (see, e.g., van der Klis 2004):

1. kHz QPOs in NS LMXBs, representing the fastest variability observed in X-ray binaries
2. Hectohertz QPOs in NS LMXBs
3. High Frequency QPOs in BH binaries
4. ms oscillations during Type I X-ray bursts in NS LMXBs
5. ms oscillations in the persistent emission of accretion-powered pulsars

All these new phenomena were discovered thanks to a dedicated timing mission, RXTE

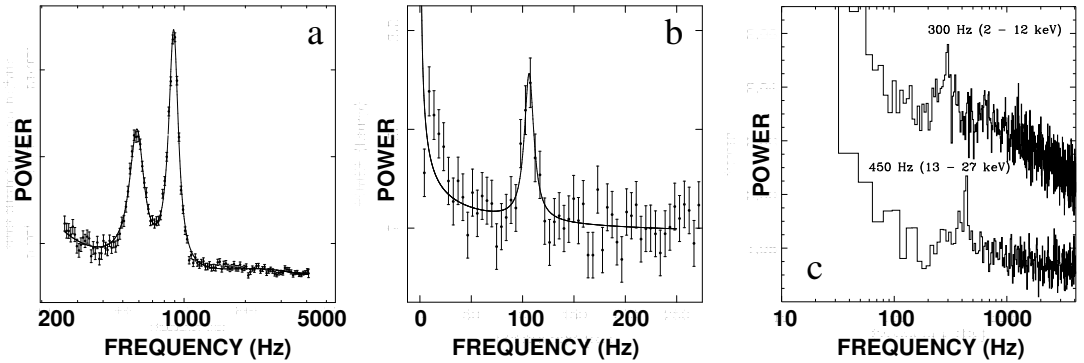

Figure 9: From van der Klis (2004). (*a*) Twin kHz QPOs in the LMXB Sco X-1 (van der klis et al. 1997). (*b*) Hectohertz QPO in the LMXB 4U 0614+09. (*c*) High frequency QPO in the BH binary GRO J1655–40 (Strohmayer 2001).

- kHz QPOs (van der Klis et al. 1996) observed in both Z and atoll sources. They manifest a rather reach phenomenology: Two peaks (usually referred to as the upper and lower kHz QPOs, ν_u and ν_l) occur in the power spectrum and move up and down in frequency together in the 200-1200 Hz range, in correlation with the source spectral state. The several 100-Hz peak separation $\Delta\nu = \nu_u - \nu_l$ is typically within 20% of the NS spin frequency, or half that, depending on source, and usually decreases by a few tens of Hz when both peaks move up by hundreds of Hz

- NS Hectohertz QPOs (Ford & van der Klis 1998) are observed only in atoll sources in most spectral states with a frequency $\nu_{hHz} = 100 \div 200$ Hz. Their frequency is approximately constant (and quite similar across sources).

- BH high frequency QPOs are the fastest variability observed in BH binaries (Remillard et al. 1999) and are observed in well defined transitionary states. As for the NS Hectohertz QPOs their frequency is approximately constant. The frequencies of these QPOs ν_{BHF} range from 100 to 450 Hz, and sometimes harmonically related frequencies have also been seen.

- ms oscillations during Type I X-ray bursts are transient phenomena observed in 10 LMXBs only during the short duration of a burst (e.g. Strohmayer et al. 1996). The frequency range of these oscillations is between 300 and 600 Hz

- ms oscillations in the persistent emission of LMXBs: coherent pulsations are detected with a frequency in the range 270-619 Hz, produced by rotational modulation of the NS emission (Wijnands & van der Klis 1998), providing a direct measurement of the NS spin frequency

Rapid variability in XRBs: interpretation

Different models try to interpret this rather complex phenomenology:

- Beat-frequency model 1 2 3 for kHz QPOs (Miller, Lamb & Psaltis 1998)
- Relativistic precession model for kHz QPOs (Stella & Vietri 1998; Stella, Vietri & Morsink 1999)
- Diskoseismic oscillations of the accretion disk for NS-Hectohertz QPOs and BH-High Frequency QPOs (Kato et al. 1998; Titarchuk et al. 1999)
- Relativistic resonance model for NS-Hectohertz QPOs and BH-High Frequency QPOs (Abramowicz & Kluźniak 2001)

In most models, one of the characteristic frequencies (usually the highest frequency of the system, e.g. the upper kHz QPO ν_u in NS systems) is identified with the Keplerian frequency ν_K at some preferred radius in the disk r_K.

In the Schwarzchild spacetime:

$$\begin{aligned} \nu_K &= (1/2\pi)(GM/r_K^3)^{1/2} \sim 1200\,\mathrm{Hz}\,(r_K/15\,\mathrm{km})^{-3/2}(M/1.4\,M_\odot)^{1/2} \\ &\sim 200\,\mathrm{Hz}\,(r_K/90\,\mathrm{km})^{-3/2}(M/10\,M_\odot)^{1/2} \quad \Longrightarrow \quad \text{ms oscillations} \end{aligned} \tag{8}$$

In the Kerr spacetime:

$$\nu_K = \pm(1/2\pi)M^{1/2}/r^{3/2}\left(1 \pm aM^{1/2}/r^{3/2}\right)^{-1} \tag{9}$$

Rapid variability in XRBs: Burst oscillations and ms oscillations in accretion-powered pulsars

- ms oscillations during Type I X-ray bursts: $\nu_{burst} = 300 - 600$ Hz

  Observed in 10 LMXBs only during the short duration of a burst (e.g. Strohmayer et al. 1996). Chakrabarty et al. (2003, Nature) firmly established burst oscillations as nuclear-powered pulsations tracing the spin of accreting NSs, corroborating earlier evidence

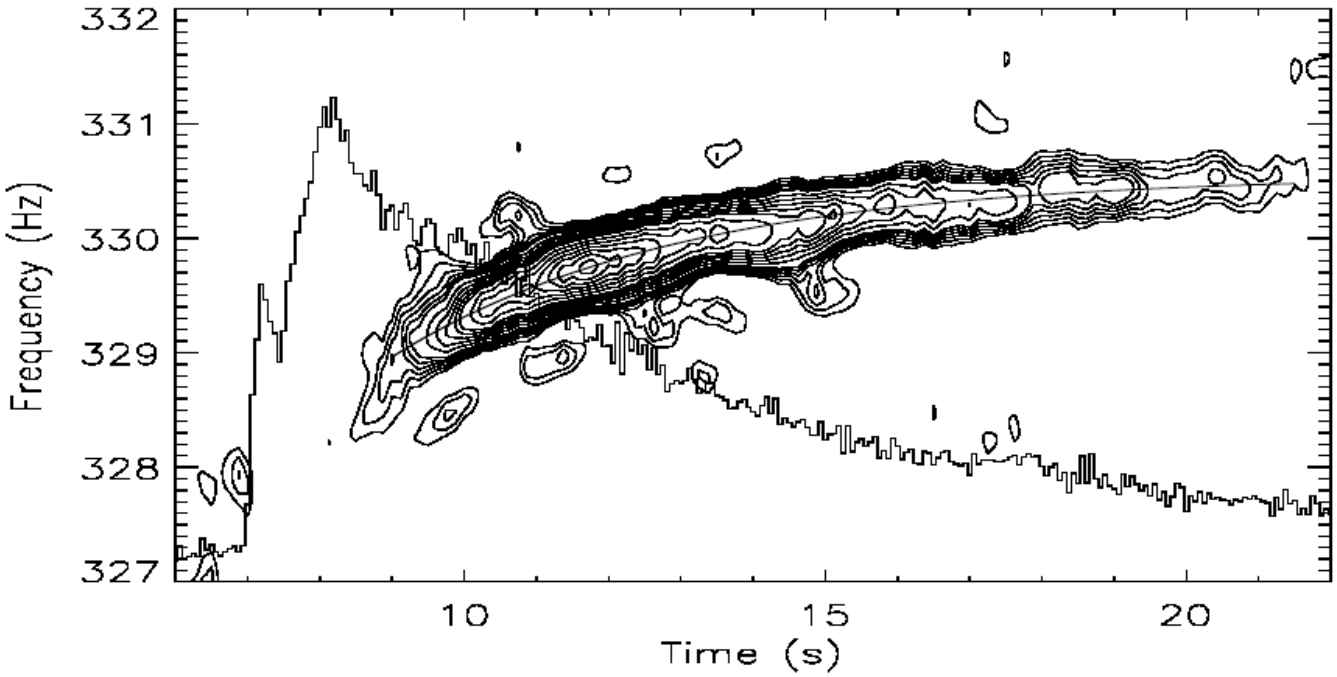

Figure 10: A dynamic power density spectrum of a burst from 4U 1702-429 showing frequency drift toward an asymptotic limit. The solid curve is a best fit using an exponential (Strohmayer 1999b).

- ms oscillations in accretion-powered pulsars: $\nu_{pulsar} = 270 - 619$ Hz

  Coherent pulsations produced by rotational modulation of the NS emission. They provide a direct measurement of the NS spin frequency. Bursts of periodic or quasi periodic variability are also observed in these sources (Wijnands et al. 2003)

  A total of 11 such objects have been identified, including **SAX J1808.4-3658**, the first acccreting ms pulsar to be discovered (Wijnands & van der Klis 1998)

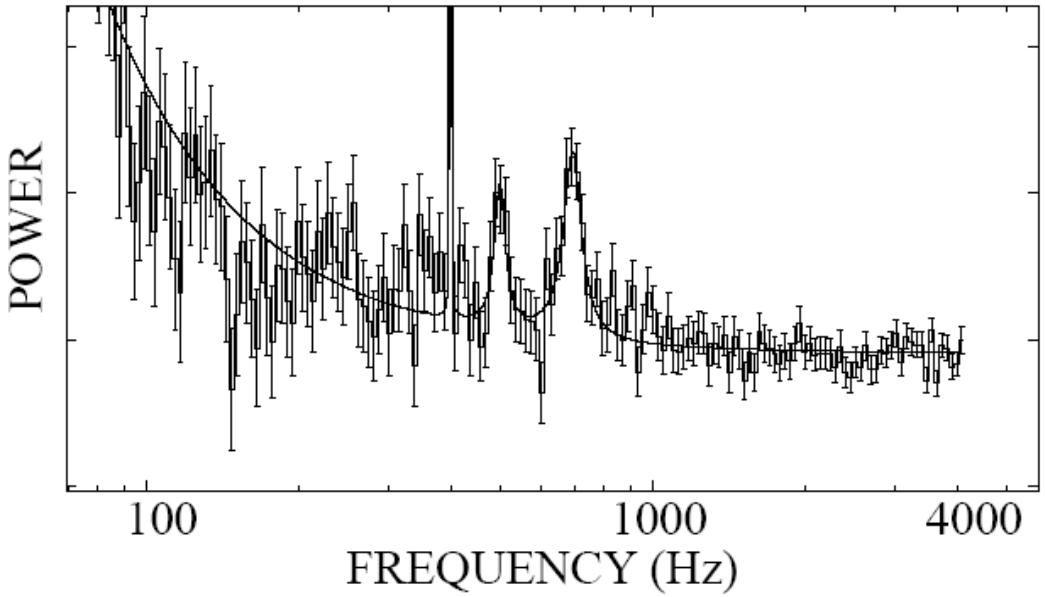

Figure 11: PDS of the accreting ms pulsar SAX J1808.4-3658, showing both the twin kHz QPOs and the 401 Hz ms oscillation (Wijnands et al. 2003; van der Klis 2004).

Rapid variability in XRBs: state of nuclear matter

- Limits on the radius-mass diagram of NSs (Miller, Lamb & Psaltis 1998)

$$\nu_K(r_{ISCO}) \propto 1/M \tag{10}$$

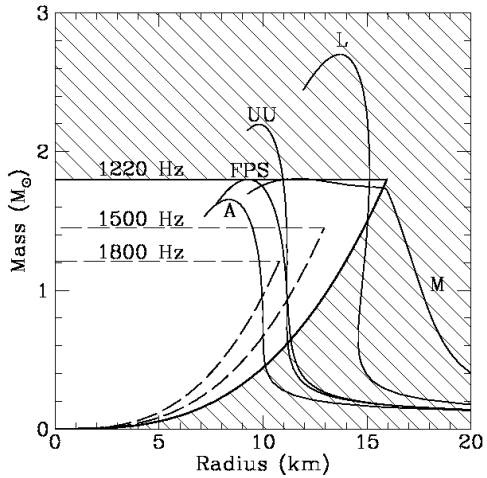

Figure 12: Comparison of the mass-radius relations for nonrotating NSs given by 5 representative equations of state for NS matter with the regions of the mass-radius plane allowed for nonrotating stars using the highest observed frequency of the higher frequency QPO in a pair. The light solid curves show the mass-radius relations given by different equations of state. (From Miller, Lamb & Psaltis 1998, ApJ).

Work taking into account the detailed structure of the NS: Morsink & Stella (1999), Marković (2000)

- Constraining the EOS

  One of the primary goals of the eXTP mission is measuring the equation of state of matter at supra-nuclear density using X-ray timing.

  eXTP will mainly use two techniques to constrain M and R for several NSs: pulse profile modeling and spin measurements.

  Constraints on the EOS can be obtained from the fastest spin rates and in particular more rapidly spinning NS place increasingly stringent constraints on the EOS. Since eXTP would have a larger effective area than any preceding X-ray timing mission, it is well suited to discover many more NS spins, using both burst oscillations and accretion-powered pulsations.

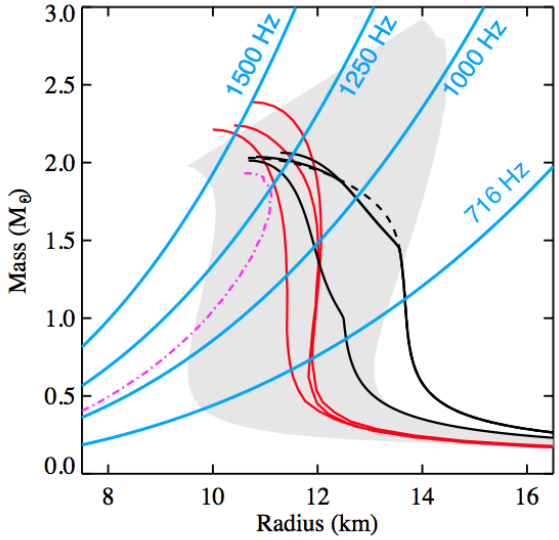

Figure 13: Spin limits on the EOS (from Watts et al. 2016).

TIMING OF ISOLATED NEUTRON STARS

Timing of isolated NSs allows us *to reconstruct their pulse shape and to track their rotational history*.

- Comparing the pulse shape at different wavelengths provides a powerful tool to locate the emission regions inside the magnetosphere and to constrain the pulsar emission mechanism, which is still not fully understood.

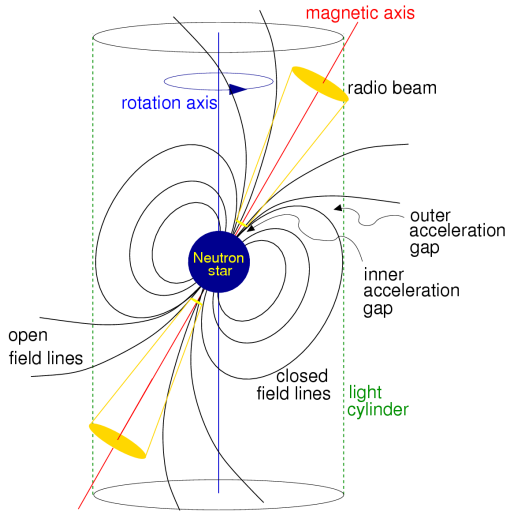

Figure 14: Magnetic dipole model of a pulsar (https://www.cv.nrao.edu/course/astr534/Pulsars.html).

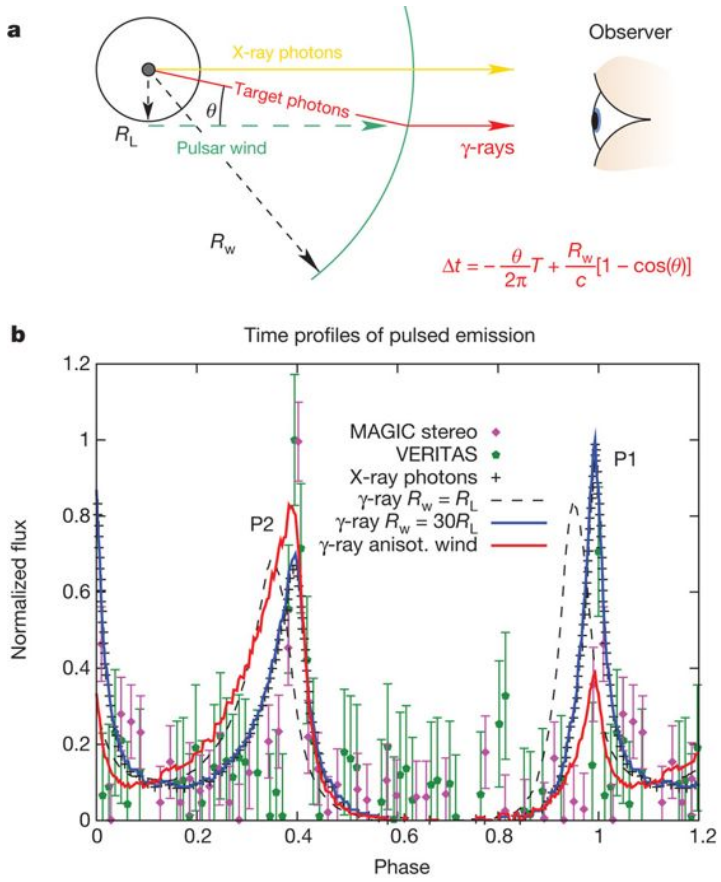

Figure 15: (a) Geometry of the inverse Compton scattering of magnetospheric X-rays by the electron-positron wind. (b) Theoretical γ-ray light curves of the wind presented together with the reported VHE data (Aharonian et al. 2012).

- The rotational history of a pulsar tells us about the mechanisms responsible for the pulsar slowdown (magnetic dipole radiation, relativistic pulsar wind; Lyne et al. 2015).

But it tells us also about possible clock irregularities (deviations from a regular slowdown known as timing noise and glitches) caused by other phenomena, such as magnetospheric instabilities (Lyne et al. 2010), NS interior readjustments (Espinoza et al. 2011), electromagnetic interaction of the pulsar with the surrounding environment (Cadez et al. 2016).

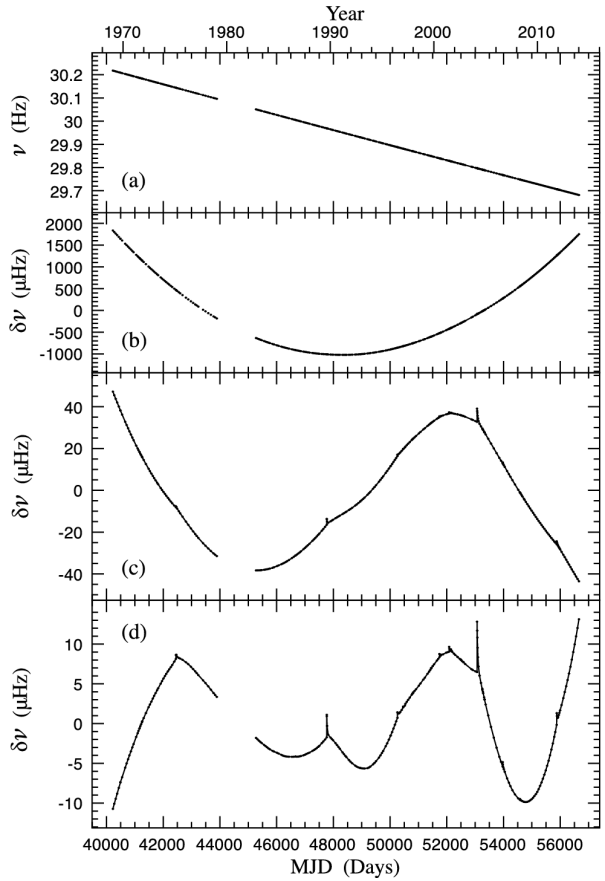

Figure 16: The spin-frequency history of the Crab pulsar over 45 years (from Lyne et al. 2015).

The implications of these studies are relevant for:

- investigating the physics of the NS interior (at nuclear densities and with very high magnetic fields)
- testing General Relativity through the timing of binary pulsars (Kramer and Stairs 2008)
- understanding the leptonic acceleration mechanisms powering pulsars and Pulsar Wind Nebulae
- detecting low frequency ($10^{-9} - 10^{-6}$ Hz) gravitational waves produced by massive black hole binaries in the centers of merging galaxies through a network of pulsars (Pulsar Timing Array; e.g. Hobbs et al. 2010)